

M³T: Discrete Multi-Modal Motion Tokens for Sign Language Production

Alexandre Symeonidis-Herzig[✉], Jianhe Low[✉],
Ozge Mercanoglu Sincan[✉], and Richard Bowden[✉]

CVSSP, University of Surrey, United Kingdom
{a.symeonidisherzig, jianhe.low,
o.mercanoglusincan, r.bowden}@surrey.ac.uk

Abstract. Sign language production requires more than hand motion generation. Non-manual features, including mouthings, eyebrow raises, gaze, and head movements, are grammatically obligatory and cannot be recovered from manual articulators alone. Existing 3D production systems face two barriers to integrating them: the standard body model provides a facial space too low-dimensional to encode these articulations, and when richer representations are adopted, standard discrete tokenization suffers from codebook collapse, leaving most of the expression space unreachable. We propose SMPL-FX, which couples FLAME’s rich expression space with the SMPL-X body, and tokenize the resulting representation with modality-specific Finite Scalar Quantization VAEs for body, hands, and face. M³T is an autoregressive transformer trained on this multi-modal motion vocabulary, with an auxiliary translation objective that encourages semantically grounded embeddings. Across three standard benchmarks (How2Sign, CSL-Daily, Phoenix14T) M³T achieves state-of-the-art sign language production quality, and on NMFs-CSL, where signs are distinguishable only by non-manual features, reaches 58.3% accuracy against 49.0% for the strongest comparable pose baseline.

Keywords: Sign Language Production · Motion Tokenization · 3D Morphable Models

1 Introduction

Producing sign language requires the coordinated generation of two articulatory channels: the manual channel, comprising hand shape, orientation, and motion, and the non-manual channel, comprising facial expression, mouthing, gaze, and head dynamics [6, 68, 71]. Critically, Non-Manual Features (NMFs) are grammatically obligatory; they negate statements, alter grammatical mood, or distinguish between otherwise identical manual signs [68]. Generating these cues faithfully is therefore essential for Sign Language Production (SLP) systems to achieve accurate and grammatically complete signing.

Despite their importance, current 3D SLP systems focus primarily on manual features or rely on low-dimensional facial models. This renders them unable to distinguish signs that share identical manual form and are differentiated solely by mouthing [71]. A system that cannot generate NMFs cannot produce these signs correctly. We identify two barriers to integrating expressive NMFs into discrete pipelines. First, a *representational*

bottleneck: the standard SMPL-X body model [51] is used with only ten expression parameters, insufficient to capture the mouthings and facial dynamics required for accurate SLP. Second, a *quantization challenge*: unlike body and hand pose, which are parameterized as geometric joint rotations over a high-variance space where even coarse codebook coverage produces plausible motion, facial expressions are encoded as low-rank PCA coefficients in a compact manifold. In this regime, each unoccupied codebook entry corresponds to an entire cluster of expressions, a mouthing, a brow raise, possibly becoming unreachable. Commonly used Vector Quantized (VQ)-Variational Autoencoder (VAE) suffer from codebook collapse in this setting, reaching only 79% utilization in our experiments and leaving significant regions of the expression space unrecoverable. The closest prior work, SOKE [98], achieves strong manual production but shares both limitations: SMPL-X’s low face parameter count and a shared VQ codebook across body and face that restricts capacity for high-dimensional facial articulation.

Motion language models [34, 83] leverage discrete tokens to give transformers the same structural advantages for motion as for text. We adopt this paradigm in M³T, resolving both barriers with three contributions. First, we construct SMPL-FX, integrating the FLAME [41] head and its 100-dimensional expression space into SMPL-X [51] to provide the representational capacity for NMFs that baselines lack. Second, we introduce modality-specific Finite Scalar Quantized (FSQ)-VAEs that tokenize body, hand, and facial motion independently. By replacing learned codebooks with fixed grids, FSQ [49] eliminates the collapse that makes VQ impractical for PCA-based face parameters, reaching 99% utilization for facial tokens. Finally, we train an autoregressive transformer on this vocabulary with an auxiliary translation objective that encourages semantically grounded embeddings, improving both geometric fidelity and back-translation quality.

Across three standard sign language benchmarks (How2Sign [18], CSL-Daily [95], Phoenix14T [7]), M³T achieves state-of-the-art production quality without external sign dictionaries. On the NMFs-CSL benchmark [29], which contains signs distinguishable only by non-manual facial features, M³T achieves 58.3% Top-1 accuracy against 49.0% for the leading pose-based baseline trained on similar data, showing that the learned tokens capture the grammatical distinctions that prior systems represent too coarsely to recover. Our results suggest that the primary barrier to linguistically complete sign production has been representational rather than architectural.

2 Related Work

Human Motion Modeling. *Motion generation*, synthesizing body motion conditioned on audio, prior motion, or text [34, 92, 98], is a long-standing problem in graphics and vision [2, 40]. Recent text-to-motion methods fall into two dominant architectures: diffusion models [26, 59, 67, 75, 87, 93], which generate continuous trajectories in latent space, and tokenized autoregressive models [34, 92, 98], which discretize motion via codebooks and train Large Language Model (LLM) backbones [45, 57]. While diffusion emphasizes motion realism, tokenized formulations cast motion as a symbolic vocabulary that a language model can directly process for both text-conditioned generation and for *motion captioning* [52, 73], the inverse task of describing motion in natural language. Prior works have trained these tasks together in shared architectures [34, 92]; while their

primary goal is task unification, the shared vocabulary can act as a semantic anchor, encouraging tokens to retain linguistically relevant features. Sign is a natural fit for tokenized motion modeling because it is a language expressed in the visual modality rather than merely movement. Representing motion as discrete tokens aligns with the inherent linguistic structure of sign. However, they pose additional challenges as fully fledged languages. Generated sign motion must satisfy grammatical constraints rather than simply appear plausible and natural, and the vocabulary cannot omit obligatory articulators such as NMFs, as this prevents linguistically correct SLP.

Sign Language Translation and Production. SLP (text-to-sign) and Sign Language Translation (SLT) (sign-to-text) are conceptually symmetric, yet largely developed in isolation [11]. SLP has progressed from rule-based and retrieval systems [24, 37, 48] to neural two-stage pipelines [64, 69], and more recently transformer- [30, 63] and diffusion-based models [3]. Across both 3D body-model pipelines and video-based rendering approaches [20, 54, 81], the incorporation of facial NMFs remains a challenge, with facial articulation largely absent from current systems regardless of the underlying representation. In 3D pose-based pipelines, a common shortcoming is the parametric body model. While SMPL-X [51] theoretically supports up to 100 expression coefficients, in practice only ten are ever used, too few to encode the mouthings and facial expressions required in sign. Conversely, SLT models map video or pose sequences to text using gloss¹-based supervision [8, 29] or end-to-end transformers [9, 78], increasingly strengthened by pretrained LLMs [13, 14, 36, 84]. While emerging SLT methods [33, 42] have begun incorporating facial cues, NMF integration in production remains underexplored.

Discrete Motion Representation. Discrete quantization underpins modern generative modeling, from images [19, 77] to motion [25, 34, 83, 92]. VQ-VAEs [58, 77] replace continuous latents with nearest codebook entries, enabling transformer-based motion generation. Sign language production has adopted VQ tokenization [80, 81, 98], but primarily for body and hand motion. When applied to high-dimensional facial parameters, VQ-VAEs suffer codebook collapse: in our experiments VQ achieves only 79% face codebook utilization, leaving large regions of the expression space unreachable. FSQ [49] removes the learned codebook entirely, partitioning the latent space into a structured grid and shifting nonlinearity into the encoder-decoder, leading to higher utilization and better reconstruction. Extending FSQ to the face modality, where codebook collapse is most severe, is the step required for discrete facial tokens to carry the full range of non-manual distinctions present in sign corpora.

3 Method

Multi-Modal Motion Tokens (M³T) is a sign language production framework (Fig. 1) built on a discrete multi-modal motion representation spanning face, body, and hands. Our framework comprises two key components: (1) a multi-modal motion FSQ-VAE tokenizer that converts the SMPL-FX parameters produced by our human reconstruction pipeline into synchronized streams of discrete tokens, providing the dense representation that enables (2) our Sign Motion Language Model (SMLM), an autoregressive

¹A gloss is a written approximation of a sign’s meaning.

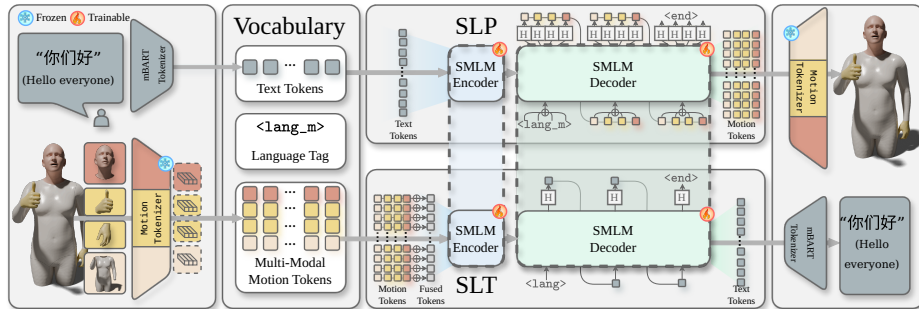


Fig. 1: Sign Motion Language Model. A single autoregressive transformer operates over SLP (text→motion) and SLT (motion→text) within a shared token space. Spoken-language tokens and modality-specific FSQ motion tokens (body, hands, face) are embedded and concatenated with boundary identifiers (e.g., <ASL_RH>, <DGS_F>) to distinguish language and articulator streams. The model predicts the next token across all modalities using a unified encoder and decoder with modality-specific output heads. An auxiliary translation objective encourages semantically grounded token embeddings, improving production quality. Both production and translation share the same encoder-decoder parameters.

transformer trained on this vocabulary for sign production, with an auxiliary translation objective that regularizes token embeddings toward semantic grounding.

A lightweight recognition module further probes the linguistic content of the resulting motion vocabulary, particularly in the context of NMFs. We begin by describing the human reconstruction process that provides the 3DMM parameters used for tokenization.

3.1 Human Reconstruction

The first stage of our pipeline extracts temporally coherent 3D Morphable Model (3DMM) parameters from monocular signing footage, providing the representation on which all downstream tokenization and generation operates. Recent monocular reconstruction advances make this tractable at scale [23, 53, 62], and large-scale extraction pipelines across continuous sign corpora have been demonstrated [3, 7, 18, 95, 98]. Sign language places a specific demand on facial representation that general body estimation does not address. Many signs share identical manual form, i.e., the same hand shape, trajectory, and location, but carry distinct meanings solely through the word being mouthed [6]. Recovering these distinctions, as well as other NMFs, requires resolving accurate facial reconstruction beyond the resolution of a low-dimensional blendshape parameterization such as the one often used in SMPL-X [51].

Fig. 2 shows SMPL-X [51] fittings used by prior 3D SLP systems [98] and the resulting inaccurate faces. While head pose is reasonably well captured, the facial parameters collapse to near-constant values across the sequence, resulting in a static face that cannot encode the NMFs required for accurate signing. A model trained on these parameters has no access to these distinctions and therefore cannot produce them.

To alleviate this, we construct *SMPL-FX*: an upper-body model that replaces SMPL-X’s head with the FLAME [41] mesh and its 100-dimensional expression space, pro-

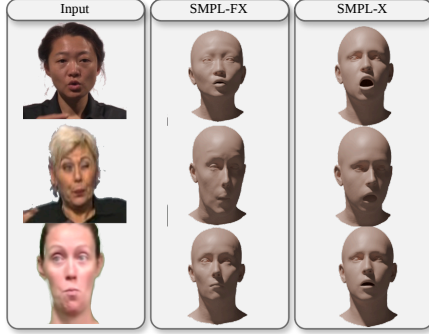


Fig. 2: SMPL-FX (ours) vs. SMPL-X. Facial parameters for SMPL-FX are extracted via Pixel3DMM [23]; for SMPL-X we use parameters as extracted by SOKE [98]. The SMPL-X captures primarily head rotation, failing to capture mouth shape and any smaller expressions.

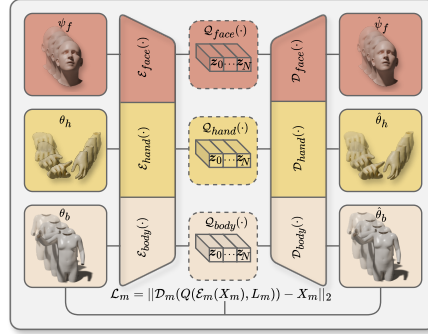


Fig. 3: Multi-modal FSQ-VAE Tokenization. Our FSQ-VAE framework discretizes modality-specific SMPL-FX latents into a structured grid. The resulting token streams provide a unified, compact, and discrete multi-modal representation specifically optimized for signing motion.

viding the resolution needed to capture mouthings and the full range of grammatically relevant NMFs. As shown in Fig. 2, SMPL-FX both captures these details and provides a more accurate head shape, useful for downstream rendering and avatar production. Since the lower body contributes minimally to signing, we retain only the torso and arms, removing 12 irrelevant joints for efficiency. Each frame of signing motion is encoded as:

$$\theta_h = \{\theta_h^l, \theta_h^r\} \in \mathbb{R}^{15 \times 6}, \theta_b \in \mathbb{R}^{10 \times 6}, \psi_f \in \mathbb{R}^{108}, \quad (1)$$

where θ_h^l and θ_h^r denote left and right hand pose, θ_b represents body pose, and ψ_f encodes facial expressions. Each pose is parameterized using the continuous 6D representation [97] for training stability, and a static identity blendshape $\beta \in \mathbb{R}^{110}$ is estimated per signer. Because θ_h and θ_b are initially estimated per frame, we further refine them across the sequence to regularize joint velocity and minimize 2D keypoint reprojection error [89]. With optimized parameters, generation of the full mesh is then performed as:

$$(\mathbf{V}, \mathbf{J}) = \text{SMPL-FX}(\beta, \theta_h, \theta_b, \psi_f), \quad (2)$$

where $\mathbf{V} \in \mathbb{R}^{N_v \times 3}$ are vertex coordinates and $\mathbf{J} \in \mathbb{R}^{N_j \times 3}$ are 3D joint locations. Operating directly in the 3DMM domain, as opposed to pose, also facilitates real-time rendering of photorealistic, sign-capable avatars [32, 79, 91] through 3D Gaussian Splatting (3DGS) pipelines. SMPL-FX further augments the face with rigidly-attached teeth geometry [55] and independent eyelid controls [23] absent from SMPL-X. To avoid neck artifacts at the FLAME-SMPL boundary, vertex positions are interpolated between SMPL-X and FLAME blend weights, weighting toward the body at the neck base and toward the face near the jawline; models are globally aligned via eye displacement following [91].

3.2 Multi-Modal Sign Motion Tokenization

Our 3DMM representation captures the tightly coordinated interactions of hands, body, and face from which sign language meaning arises. However, these continuous parameters remain high-dimensional and irregular, making them ill-suited for sequence-to-sequence modeling. To expose their underlying compositional structure to a transformer, we discretize each articulator stream into its own symbolic vocabulary using modality-specific FSQ-VAEs [49] (Fig. 3). This converts trajectories into informationally dense token streams that preserve the body motion, hand articulation, and non-manual facial expressions required to represent the full linguistic content of signing.

Encoders: For each modality $m \in \{b, h, f\}$, we encode the 3DMM sequences $X_m \in \mathbb{R}^{T \times D_m}$ of T frames and dimension D_m (Eq. (1)) using a stack of 1D convolutional residual blocks [34], enabling aggregation of motion cues while compressing temporally. This produces downsampled latents, with window size w and latent dimension d :

$$Z_m = \mathcal{E}_m(X_m) \in \mathbb{R}^{\frac{T}{w} \times d}. \quad (3)$$

Left hand poses are mirrored before encoding, enabling a shared hand encoder.

Quantization: Applying VQ-VAE to the facial stream $\psi_f \in \mathbb{R}^{108}$ produces codebook collapse, particularly as faces are parameterized via low-rank PCA coefficients rather than geometric pose angles. As discussed in later sections, our experiments reveal that VQ-VAE reaches only 79% codebook utilization, leaving significant manifolds of the expression space unreachable and rendering discrete facial tokenization representationally bottlenecked. FSQ [49] resolves this by independently mapping each dimension i of Z_m into a predefined level $[0, L_m^i - 1]$ ($L_m \in \mathbb{Z}^d$), via the element-wise quantization, with rnd_{ste} denoting straight-through estimation [4] rounding for gradient flow:

$$\hat{Z}_m = Q(Z_m, L_m) = \text{rnd}_{\text{ste}} \left(\frac{L_m}{2} \tanh(Z_m) \right). \quad (4)$$

Unlike VQ-VAE [77], FSQ does not require a learned codebook or a commitment loss, eliminating the risk of codebook collapse and improving utilization of the discrete space. Deterministic quantization shifts the representational burden onto the encoder and decoder, enabling highly compact latent dimensionalities while maintaining high-fidelity reconstruction. Quantization enables us to represent each window of w frames as a single discrete integer index selected from an implicit codebook of size $C_m = \prod_{i=1}^d L_m^i$. This yields $\hat{Z}_m \in \{1, \dots, C_m\}^{\frac{T}{w}}$ as a concise, modality-aligned sequence of motion tokens.

Decoder: The tokens \hat{Z}_m can then be decoded using modality-specific decoders $\mathcal{D}_m(\cdot)$, whose structure mirrors that of the encoders, to reconstruct the 3DMM parameters.

$$\hat{X}_m = \mathcal{D}_m(\hat{Z}_m). \quad (5)$$

As we employ FSQ, training seeks to minimize the ℓ_2 reconstruction error across modalities without the need for auxiliary codebook losses or commitment terms:

$$\mathcal{L}_m = \|\mathcal{D}_m(Q(\mathcal{E}_m(X_m), L_m)) - X_m\|_2. \quad (6)$$

Once trained, each modality-specific FSQ-VAE provides discrete tokens that preserve the detailed articulations and expressions. Together, these modality-specific FSQ-VAEs form

a comprehensive discrete multi-modal representation spanning the full body, both hands, and an expressive face. This provides the model with a vocabulary that can capture the full range of linguistic distinctions in signing, including those conveyed by NMFs, while remaining compact and structured for efficient sequence modeling in our SMLM.

3.3 Sign Motion Language Model

Using these multi-modal motion FSQ-VAEs, we project motion trajectories into a sequence of sign tokens in the same embedding space as a pre-trained language model [45] text vocabulary \mathcal{V}_t . We construct a sign vocabulary per modality by introducing a unique “word” for every FSQ index: $\mathcal{V}_m = \{\langle m_1 \rangle, \dots, \langle m_C_m \rangle\}$. As is standard for multi-lingual models [45, 98], we define language tokens $\mathcal{V}_l = \{\langle \text{lang_m} \rangle\}$ for each combination of language and modality. These tags serve as domain prompts, allowing the same model to handle multiple languages. Explicitly decoupling the hands yields four sign modalities $m \in \{b, lh, rh, f\}$, which when combined with pre-existing text and new language-modality tokens, produce our language model’s complete lexicon:

$$\mathcal{V} = \mathcal{V}_t \cup \mathcal{V}_l \cup \mathcal{V}_b \cup \mathcal{V}_{lh} \cup \mathcal{V}_{rh} \cup \mathcal{V}_f. \quad (7)$$

Sign Language Production: Given a sequence of spoken-language text \mathbf{S} , the unified multi-modal vocabulary allows the model to autoregressively generate a sequence of sign-motion tokens $\mathbf{Y} = \{y_u\}_{u=1}^U$, where each time step contains one token per modality. The input text sequence is first embedded and encoded by the transformer encoder. Its final hidden states condition the decoder, which predicts the next multi-modal token set:

$$P(\mathbf{Y} | \mathbf{S}) = \prod_{u=1}^U P(y_u | y_{<u}, \mathbf{S}). \quad (8)$$

To adapt the decoder to multi-modal generation, we follow [98] and prepend modality-specific language prompts (e.g., $\langle \text{ASL_LH} \rangle$, $\langle \text{DGS_F} \rangle$) to \mathbf{Y} . Because the decoder expects a single input token per time step, we fuse the embeddings of the current step’s motion tokens via an equal-weight average. Concatenation would scale the effective sequence length by the number of modalities and we empirically found a learned fusion layer to introduce training instabilities. Since all four modalities describe the same temporal instant, we opt for equal-weight aggregation as per-modality discrimination is deferred entirely to the output heads.

For output, the transformer’s hidden state is routed through parallel modality-specific linear heads, where each head predicts only the logits for its modality’s vocabulary using the decoder’s last hidden state. This avoids computationally expensive sequential prediction across modalities and therefore provides a more efficient decoding, while still enabling all heads to share the transformer’s semantic and temporal structure. The result is a decoder that simultaneously produces body, left hand, right hand, and face tokens with fine control and cross-modal coherence.

Auxiliary Translation Objective: Prior work has observed that sign-to-text supervision encourages more semantically grounded sign representations [74, 79]. We incorporate this as an auxiliary training objective to regularize the motion generation: given the

motion-token streams \mathbf{Y} , their embeddings are fused and passed to the encoder, and the decoder autoregressively predicts the spoken-language sequence $\mathbf{S} = \{s_k\}_{k=1}^K$:

$$P(\mathbf{S} | \mathbf{Y}) = \prod_{k=1}^K P(s_k | s_{<k}, \mathbf{Y}) \quad (9)$$

using a single shared output head over the shared spoken-language vocabulary. The translation loss serves as a semantic regularizer that further organizes the motion-token embedding space according to linguistic content, encouraging the encoder to cluster tokens whose underlying signs share meaning. The resulting semantic grounding consistently improves geometric fidelity and back-translation quality.

Both objectives use standard cross-entropy losses. During training, we alternate them by randomly sampling ($p = 0.5$) production or translation per batch. In the multi-stream setting, generation terminates when any modality emits the $\langle \text{EOS} \rangle$ token. At inference time, we employ greedy decoding, selecting the most probable token at each step. For motion outputs, predicted discrete tokens are mapped back to 3DMM parameters using the frozen FSQ-VAE decoders, allowing mesh generation via Eq. (2). These meshes can be rendered into signing videos using 3DGS-based avatar synthesis [32, 38, 55, 72].

3.4 Sign Language Recognition

Sign Language Recognition (SLR) maps video clips of isolated lexical signs to discrete class labels. In the context of M³T, we do not treat SLR as an end goal, but rather as a diagnostic tool to evaluate the representational fidelity of our learned multi-modal motion tokens. Standard continuous metrics such as joint position error cannot fully capture whether vital components of sign, both manual and non-manual, have been preserved. By evaluating SLR on subsets of signs that are manually identical but distinguishable by NMFs, we can assess the semantic richness and discriminative power of our tokens.

To isolate the quality of the representation, our modality-specific FSQ-VAE encoders remain frozen during this phase. Following [86], we first isolate the active signing window for each sequence \mathbf{Y} by applying thresholds on hand height and displacement relative to a neutral rest pose, trimming uninformative initial and final frames. The temporally cropped frames are then processed by the frozen body, hand, and face encoders. We extract the final high-dimensional continuous hidden states immediately preceding the FSQ quantization step. These modality-specific feature sequences are interleaved across modalities to form a structured temporal sequence, which is fed into a transformer encoder to capture global temporal dependencies, followed by a linear MLP classification head that predicts the sign class.

The classifier is trained using cross-entropy with label smoothing. Because the underlying motion encoders are frozen, the downstream SLR accuracy acts as a direct proxy for representation quality. High performance on confusing signs, where manual features are identical and only face tokens carry discriminative information, suggests that SMPL-FX captures the mouthing and expression distinctions required for NMFs and that FSQ encodes these facial dynamics into powerful discrete tokens.

4 Experiments

We investigate whether our discrete multi-modal tokens constitute a motion representation capable of driving SLP via three experiments: production quality on standard continuous sign benchmarks (Sec. 4.2), representational fidelity of facial tokens on the NMFs-CSL isolated sign recognition benchmark (Sec. 4.3), and tokenization design choices via ablation (Sec. 4.4). Together, these experiments test whether the SMPL-FX representation and FSQ tokenization produce motion tokens that are both geometrically accurate and linguistically discriminative, particularly for the facial channel that prior systems leave largely static.

4.1 Experimental Setup

Datasets: We evaluate on three continuous sign datasets frequently used in both SLP and SLT: How2Sign [18] (American Sign Language (ASL), 30K sentences), CSL-Daily [95] (Chinese Sign Language (CSL), 20K sentences), and Phoenix14T [7] (German Sign Language (DGS), 8K sentences). To aid expressive modeling of NMFs, the face FSQ is additionally trained with FLAME parameters from MEAD [82], as extracted by [17].

To directly measure generalization of facial cues, we further evaluate SLR performance on the specialized NMFs-CSL [29]. This benchmark contains 32K isolated signing videos spanning 610 “confusing” signs that are distinguishable only through NMF, along with 457 “normal” signs, making it a useful test for the representational fidelity, particularly for NMFs, of our multi-modal motion tokens.

Training Overview: Each FSQ-VAE modality is trained independently, and the three trained models are subsequently frozen for all downstream tasks. Codebook sizes are selected to fairly compare with prior works at $|C_b| = 100$, $|C_h| = 180$, $|C_f| = 216$, with a dimension of $C = 3$ for all modalities at a temporal downsampling factor of $4\times$. This greatly reduced dimensionality is a common trait of FSQ, as learning is pushed from the learned high dimensional codebook entries into the encoder and decoder.

The unified transformer backbone is based on mBART-large [45], adapted to jointly process text and our motion vocabularies using shared encoder and decoder with a linear layer per output modality. Recognition is trained separately using a smaller transformer encoder and an MLP. Additional architectural specifications, hyperparameter, and implementation details for each model are provided in the appendix.

Metrics: We evaluate sign language production using standard metrics from 3D human motion generation. Geometric fidelity, body and hand accuracy are measured using mean joint position error (JPE), computed both before and after rigid alignment via *Procrustes Analysis*. For generated sequences the joints are temporally aligned with *Dynamic Time Warping* (DTW) [61]. To capture semantic preservation, we perform back-translation [65], where generated motion is translated back into text using separate SLT models. We report BLEU-4 [50] and ROUGE-L [43], the standard translation metrics, to quantify linguistic consistency between the generated and reference sentences.

As back-translation models differ across methods, we train a common [30, 65, 66, 79] transformer-based SLT model [9] on ground-truth 3DMM parameters to provide a consistent evaluation baseline. We additionally report an upper bound obtained by passing ground-truth 3DMM parameters through the same back-translation models.

Quantitative face comparison across methods is not directly feasible: each system extracts facial pseudo-GT using a different pipeline and body model, so there is no shared facial ground truth against which generated faces can be fairly evaluated. Consequently, facial assessment is primarily qualitative (Fig. 4), however, as evidenced in Fig. 2, prior methods exhibit a fundamental representational bottleneck that precludes the generation of semantically meaningful NMFs.

4.2 Evaluation on Sign Language Production

Method	How2Sign				CSL-Daily				Phoenix14T			
	DTW-PA-JPE↓		DTW-JPE↓		DTW-PA-JPE↓		DTW-JPE↓		DTW-PA-JPE↓		DTW-JPE↓	
	Body	Hand										
NAR [♦] [31]	13.94	11.80	–	–	–	–	–	–	–	–	–	–
Prog. Trans. [◇] [65]	14.15	11.57	14.74	30.17	15.98	12.91	16.30	32.63	13.67	11.95	15.01	31.77
Text2Mesh [◇] [70]	13.99	13.47	15.50	32.97	13.47	12.10	13.76	30.37	13.48	12.06	14.04	31.64
Adv. Train. [♦] [63]	13.78	11.17	–	–	–	–	–	–	–	–	–	–
T2S-GPT [◇] [90]	11.48	6.39	12.65	18.44	11.94	5.93	12.32	15.43	10.38	6.47	11.65	19.09
NSA [3]	7.83	7.33	–	–	–	–	–	–	–	–	–	–
S-MotionGPT [34] [†]	11.23	4.39	12.41	13.74	10.81	3.78	11.58	11.31	9.45	3.41	10.42	9.08
SOKE [‡] [98]	6.82	2.35	7.75	10.08	6.24	1.71	7.38	9.68	4.77	1.38	6.04	7.72
M ³ T _{w/o} SLT	4.52	2.42	5.02	8.94	4.13	1.59	4.77	9.94	3.54	1.54	4.17	9.14
M ³ T _{w/SLT}	4.28	2.28	4.86	9.44	3.97	1.51	4.63	9.28	3.41	1.46	4.02	8.55

Table 1: Comparison with state-of-the-art SLP (text-to-sign) methods. DTW-PA-JPE measures pose-aligned joint error after rigid normalization, while DTW-JPE measures raw joint position error. All metrics are computed with dynamic time warping to account for temporal variation; lower values indicate higher motion fidelity. Metrics marked with [♦] and [◇] are reported from [3] and [98] respectively. [†] is MotionGPT [34] as trained by [98] per sign dataset. [‡] SOKE uses retrieval-augmented generation with external isolated sign dictionaries; M³T achieves superior results without external retrieval or lexicon supervision.

Quantitative Comparison: Our method achieves state-of-the-art geometric SLP performance across three benchmarks (Tab. 1). We outperform both non-tokenized [3] and tokenized baselines, with substantial gains in body motion across all datasets. Notably, SOKE [98] incorporates retrieval-augmented generation [12] and benefits from additional isolated sign dictionaries; our method achieves superior results without external retrieval or lexicon supervision while also modeling the full facial expression space.

The improvements vary across datasets. On How2Sign (ASL, 30K sentences) and CSL-Daily (CSL, 20K sentences), body DTW-PA-JPE drops by 37% and 36% respectively versus SOKE, with consistent hand improvements. Phoenix14T (DGS, 8K sentences) is the smallest and oldest dataset, with lower video quality that constrains pseudo-GT extraction fidelity; gains here are accordingly more modest (body -29% versus SOKE), and the auxiliary translation objective yields smaller back-translation improvements (Phoenix: +4.1% BLEU-4; CSL-Daily: +22.4% BLEU-4; Tab. 2), consistent with the noisier signal available at training time. The +22.4% BLEU-4 gain on CSL-Daily reflects its 20K sentence-pairs providing a dense, consistent supervision

signal across all token modalities simultaneously; Phoenix14T’s noisier pseudo-GT and smaller size weaken this signal at every level. Geometric error captures body and hand motion fidelity, but does not reflect the most significant representational gap between systems: the face channel, where prior methods produce near-static outputs. On our SMPL-FX fittings, M³T achieves face DTW-VPE of **1.85**, **1.91**, and **2.23** on How2Sign, CSL-Daily, and Phoenix14T respectively. No prior 3D SLP method reports comparable face-specific production metrics. We structure our facial evaluation across three complementary lenses: reconstruction fidelity via the FSQ ablation (Sec. 4.4), semantic discriminability on NMFs-CSL (Sec. 4.3), and qualitative comparison (Fig. 4).

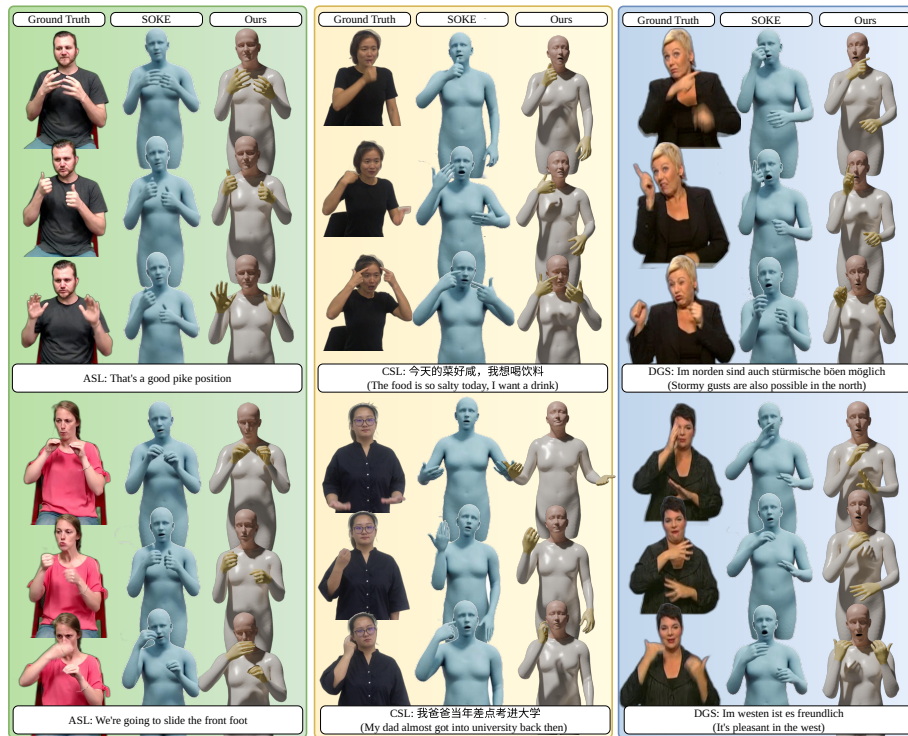


Fig. 4: Qualitative comparisons with SOKE [98] over How2Sign (left), CSL-Daily (middle), and Phoenix14T (right). SOKE’s facial outputs are largely static: jaw position and facial expression change minimally across frames and do not track the utterance, a direct consequence of SMPL-X’s ten-dimensional face space. M³T generates NMFs that vary with the signing content.

Qualitative Comparison: Figure 4 compares M³T against SOKE [98]. As shown, SOKE produces largely static facial outputs; jaw position and facial expressions remain nearly constant across frames regardless of the input utterance. This is a direct consequence of relying on SMPL-X’s highly constrained 10-dimensional facial space, which collapses distinct NMFs into indistinguishable blendshapes. In contrast, M³T generates dynamic,

Method	How2Sign		CSL-Daily		Phoenix14T	
	R \uparrow	B4 \uparrow	R \uparrow	B4 \uparrow	R \uparrow	B4 \uparrow
GT 3DMM	18.68	2.04	27.14	7.11	35.83	11.84
M ³ T _{w/o SLT}	12.32	1.58	17.27	4.74	31.14	10.16
M ³ T _{w/SLT}	13.15	1.72	20.23	5.80	32.12	10.58

Table 2: SLP Back-Translation Results. Text metrics are ROUGE-L (R) and BLEU-4 (B4). BT scores on ground truth 3DMM parameters given to highlight upper bound of results.

$Q(\cdot)$	BS	HS	PA-VPE \downarrow			Codebook % \uparrow		
			Body	Hand	Face	Body	Hand	Face
QUANTIZATION METHOD								
VQ	16	1024	20.67	5.61	1.35	67.3	72.5	78.8
FSQ	16	1024	16.11	4.94	1.18	96.4	98.1	99.0
HYPERPARAMETER SEARCH								
FSQ	128	1024	24.85	6.52	1.55	84.1	86.9	89.3
FSQ	64	1024	21.73	5.98	1.42	89.7	92.4	94.1
FSQ	32	1024	18.92	5.37	1.30	93.2	95.7	97.0
FSQ	16	512	17.03	5.12	1.08	94.9	97.2	99.5
FSQ	16	2048	16.84	4.98	1.22	97.1	98.5	99.3
FSQ	16	1024	16.11	4.94	1.18	96.4	98.1	99.0

Table 3: Ablation of Quantization Method and Parameters. Results are averaged across datasets. Lower PA-VPE indicates more accurate reconstruction; higher codebook usage reflects more efficient token utilization.

coordinated NMFs that meaningfully vary with the signing content. Because NMFs are grammatically obligatory to convey negation or alter grammatical form, their successful generation allows M³T to achieve a level of linguistic completeness absent in prior methods that primarily focus on manual production.

While M³T significantly advances facial expressivity, we observe some residual limitations. Facial outputs occasionally exhibit artifacts under severe occlusion or motion blur. Furthermore, rapid finger movements remain challenging, particularly on the How2Sign dataset, which features frequent fingerspelling. We attribute this primarily to the 4 \times temporal downsampling in our VAE encoders, rather than a fundamental limitation of the autoregressive modeling. Finally, we note a tendency for the model to spatially compress the signing space, occasionally regressing hand motions toward the center of the body.

4.3 Evaluation on Sign Language Recognition

The NMFs-CSL benchmark is designed to isolate the contribution of face tokens by contrasting two sign subsets: 457 “normal” signs that are disambiguated by manual

Method	Overall		Conf.		Norm.	
	T-1 \uparrow	T-5 \uparrow	T-1 \uparrow	T-5 \uparrow	T-1 \uparrow	T-5 \uparrow
RGB-BASED METHOD						
3D-R50 [56]	62.1	82.9	43.1	72.4	87.4	97.0
DNF [16]	55.8	82.4	51.9	71.4	86.3	97.0
I3D [10]	64.4	88.0	47.3	81.8	87.1	97.3
TSM [44]	64.5	88.7	42.9	81.0	93.3	99.0
SlowFast [21]	66.3	86.6	47.0	77.4	92.0	98.9
GLE-Net [29]	69.0	88.1	50.6	79.6	93.6	99.3
HMA [28]	64.7	91.0	42.3	84.8	94.6	99.3
NLASLR [99] \dagger	83.1	98.3	–	–	–	–
SignRep [86] \dagger	84.1	98.8	–	–	–	–
POSE-BASED METHOD						
ST-GCN [88]	59.9	86.8	42.2	79.4	83.4	96.7
SignBERT [27]	67.0	95.3	46.4	92.1	94.5	99.6
BEST [94]	68.5	94.4	49.0	90.3	94.6	99.7
ScalingUp [96] \dagger	80.2	97.5	67.2	95.7	97.5	99.8
M ³ T	74.1	95.1	58.3	93.0	93.5	97.6

Table 4: SLR results on NMFs-CSL [29], separated by RGB and pose modalities. \dagger denotes pre-training on large sign datasets. NLASLR [99] was trained with both RGB and additional pose input. *Confusing* and *normal* refer to signs distinguished solely by non-manual features and those that can otherwise be disambiguated, respectively.

features, and 610 “confusing” signs that share identical manual components and differ only in facial expression. On the normal subset, M³T scores 93.5% Top-1, marginally below BEST [94] at 94.6%. This slight variance is expected; because these standard signs are fully distinguished by hand shape and trajectory, adding face tokens provides no discriminative advantage and may marginally dilute the manual signal. On the confusing subset, where face tokens are the sole source of discriminative information, M³T achieves 58.3% against 49.0% for BEST [94]. Since body and hand features carry no discriminative signal for confusing signs, the performance gap reflects entirely the face tokens’ ability to encode grammatically relevant non-manual distinctions that prior systems often represent too coarsely to recover. Methods such as ScalingUp [96] achieve higher overall accuracy by leveraging large-scale pose pre-training on external sign corpora (e.g., YouTubeASL [76], BOBSL [1]) with recognition-optimized architectures. Our encoders are frozen production encoders, never trained for recognition; the SLR probe serves purely as a representational diagnostic. Against BEST [94], the strongest baseline without external pre-training, M³T achieves a +9.3 pp gain on the confusing subset, confirming that the face tokens encode discriminative NMF information. Importantly, the frozen encoders used in this recognition experiment are identical to those that tokenize training data for the production model. The confusing-sign accuracy is therefore a lower bound on the facial information available to the production model when generating sign with accurate NMFs.

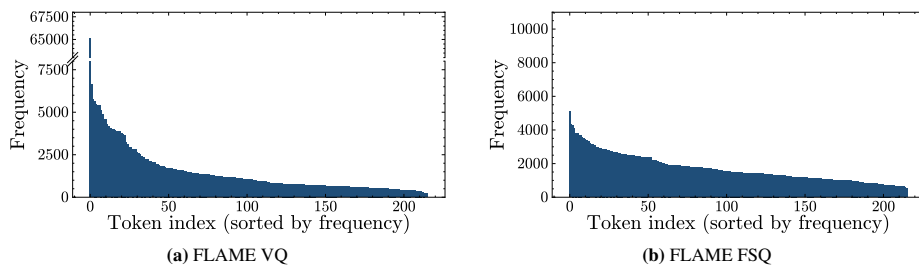


Fig. 5: Face token frequency distributions. VQ produces a heavily skewed distribution — most face codes are unused, a handful dominate — while FSQ yields more uniform coverage. Rarely-used tokens receive insufficient gradient signal, undermining the auxiliary translation objective’s ability to ground face embeddings semantically; FSQ’s structured grid eliminates this bottleneck.

4.4 Tokenization Ablation

We ablate our tokenization framework across quantization methods and architectural hyperparameters, evaluating reconstruction fidelity via PA-VPE and codebook utilization.

As detailed in Tab. 3, FSQ improves codebook utilization and reconstruction fidelity across all three modalities. Body VQ utilization is the lowest in absolute terms (67.3%), and the transition to FSQ yields the largest absolute gain there (+29.1 points to 96.4%). The 99.0% face utilization is nevertheless the critical recovery for SLP. Body and

hand parameters are geometric joint rotations over a high-variance pose space; even coarser codebook coverage produces physically plausible motion. The facial stream $\psi_f \in \mathbb{R}^{108}$ is parameterized via PCA expression coefficients. This is a compact, low-variance space where an unoccupied token corresponds to an entire facial expression cluster (a mouthing, a brow raise) becoming permanently unreachable instead of being approximated less accurately. FSQ’s near-complete face coverage therefore helps the grammatically obligatory NMFs survive tokenization, whereas VQ risks discarding them. Overall, FSQ reduces reconstruction error by 15.5% across all modalities; token frequency distributions in Fig. 5 illustrate how VQ concentrates probability mass on a smaller subset of face codes while FSQ achieves more uniform coverage. Codebook sizes are fixed at $|C_b|=100$, $|C_h|=180$, and $|C_f|=216$ to match prior work [98]; the face codebook is larger to accommodate FLAME’s higher-dimensional expression space.

Increasing the encoder hidden width (HS) to 1024 provides the most robust performance across the full skeletal structure. A smaller width of 512 achieves peak facial fidelity (1.08 PA-VPE, 99.5% utilization) but lacks the capacity to model the higher-variance dynamics of the body, resulting in a significantly higher body error of 17.03. Expanding to HS=2048 yields the highest body utilization (97.1%) but offers diminishing returns for the face. FSQ performance is also sensitive to batch size, with reconstruction quality degrading as BS increases from 16 to 128, an effect we attribute to early convergence to a subset of codes even in the absence of a learned codebook.

5 Conclusion

Facial non-manuals carry grammatical weight that manual articulation alone cannot convey. M³T brings their synthesis within reach by replacing SMPL-X’s ten-dimensional face model with FLAME’s 100-dimensional expression space (SMPL-FX) and resolving the codebook collapse that previously made face tokenization impractical via FSQ (99% utilization vs. 79% for VQ), yielding a discrete multi-modal representation covering the primary articulatory channels of sign. An autoregressive production model trained on this vocabulary achieves state-of-the-art results across three benchmarks, with an auxiliary translation objective further improving production quality (+3.8% JPE, +11.8% back-translation BLEU-4, +9.0% ROUGE-L) by encouraging semantically grounded token embeddings. Recognition experiments on NMFs-CSL confirm that the facial tokens encode the distinctions in NMFs that prior systems represent too coarsely to discriminate, without large-scale pre-training.

A few constraints bound the current system. Reconstruction quality degrades under occlusion and low-quality footage, and fingerspelling remains challenging under 4× temporal compression. Back-translation and joint position error are imperfect proxies for communicative quality, limitations shared by existing 3D SLP methods.

Overall, our results indicate that a primary barrier to linguistically complete sign production has been representational rather than architectural. By enabling high-capacity, collapse-free facial tokenization, M³T makes expressive SLP tractable within a discrete motion language modeling framework. Further, our SMPL-FX fittings can serve as a shared facial ground truth for future evaluation.

Acknowledgements

This work was supported by the SNSF project 'SMILE II' (CRSII5 193686), the Innosuisse ICT Flagship (PFFS-21-47), EPSRC grant APP24554 (SignGPT-EP/Z535370/1), and through funding from Google.org via the AI for Global Goals scheme. This work reflects only the author's views and the funders are not responsible for any use that may be made of the information it contains.

References

1. Albanie, S., Varol, G., Momeni, L., Bull, H., Afouras, T., Chowdhury, H., Fox, N., Woll, B., Cooper, R., McParland, A., et al.: BBC-oxford british sign language dataset. arXiv preprint arXiv:2111.03635 (2021)
2. Badler, N.I., Phillips, C.B., Webber, B.L.: *Simulating Humans: Computer Graphics, Animation, and Control*. Oxford University Press (09 1993). <https://doi.org/10.1093/oso/9780195073591.001.0001>, <https://doi.org/10.1093/oso/9780195073591.001.0001>
3. Baltatzis, V., Potamias, R.A., Ververas, E., Sun, G., Deng, J., Zafeiriou, S.: Neural sign actors: a diffusion model for 3d sign language production from text. In: *Proceedings of the IEEE/CVF Conference on Computer Vision and Pattern Recognition*. pp. 1985–1995 (2024)
4. Bengio, Y., Léonard, N., Courville, A.: Estimating or propagating gradients through stochastic neurons for conditional computation. arXiv preprint arXiv:1308.3432 (2013)
5. Blanz, V., Vetter, T.: A Morphable Model for the Synthesis of 3D Faces. In: *Proceedings of the 26th Annual Conference on Computer Graphics and Interactive Techniques (SIGGRAPH)*. pp. 187–194 (1999)
6. Boyes Braem, P., Sutton-Spence, R.: *The Hands Are The Head of The Mouth. The Mouth as Articulator in Sign Languages*. Hamburg: Signum Press (2001)
7. Camgoz, N.C., Hadfield, S., Koller, O., Ney, H., Bowden, R.: Neural sign language translation. In: *Proceedings of the IEEE Conference on Computer Vision and Pattern Recognition (CVPR)*. pp. 7784–7793 (Jun 2018)
8. Camgoz, N.C., Hadfield, S., Koller, O., Ney, H., Bowden, R.: Neural sign language translation. In: *CVPR* (2018)
9. Camgoz, N.C., Koller, O., Hadfield, S., Bowden, R.: Sign language transformers: Joint end-to-end sign language recognition and translation. In: *Proceedings of the IEEE/CVF conference on computer vision and pattern recognition*. pp. 10023–10033 (2020)
10. Carreira, J., Zisserman, A.: Quo vadis, action recognition? a new model and the kinetics dataset. In: *proceedings of the IEEE Conference on Computer Vision and Pattern Recognition*. pp. 6299–6308 (2017)
11. Chaudhary, L., Ananthanarayana, T., Hoq, E., Nwogu, I.: Signnet ii: A transformer-based two-way sign language translation model. *IEEE Transactions on Pattern Analysis and Machine Intelligence* **45**(11), 12896–12907 (2022)
12. Chen, J., Lin, H., Han, X., Sun, L.: Benchmarking large language models in retrieval-augmented generation. In: *Proceedings of the AAAI Conference on Artificial Intelligence*. vol. 38, pp. 17754–17762 (2024)
13. Chen, Y., Wei, F., Sun, X., Wu, Z., Lin, S.: A simple multi-modality transfer learning baseline for sign language translation. In: *CVPR*. pp. 5120–5130 (2022)
14. Chen, Y., Zuo, R., Wei, F., Wu, Y., Liu, S., Mak, B.: Two-stream network for sign language recognition and translation. In: *NeurIPS* (2022)

15. Contributors, M.: Openmmlab pose estimation toolbox and benchmark. <https://github.com/open-mmlab/mmpose> (2020)
16. Cui, R., Liu, H., Zhang, C.: A deep neural framework for continuous sign language recognition by iterative training. In: TMM. vol. 21 (2019)
17. Daněček, R., Chhatre, K., Tripathi, S., Wen, Y., Black, M., Bolkart, T.: EMOTE: Emotional Speech-Driven Animation with Content-Emotion Disentanglement. In: SIGGRAPH Asia 2023 Conference Papers. pp. 1–13 (2023)
18. Duarte, A., Palaskar, S., Ventura, L., Ghadiyaram, D., DeHaan, K., Metze, F., Torres, J., Giro-i Nieto, X.: How2sign: a large-scale multimodal dataset for continuous american sign language. In: CVPR. pp. 2735–2744 (2021)
19. Esser, P., Rombach, R., Ommert, B.: Taming transformers for high-resolution image synthesis. In: Proceedings of the IEEE/CVF conference on computer vision and pattern recognition. pp. 12873–12883 (2021)
20. Fang, S., Sui, C., Zhou, Y., Zhang, X., Zhong, H., Tian, Y., Chen, C.: Signdiff: Diffusion model for american sign language production. In: 2025 IEEE 19th International Conference on Automatic Face and Gesture Recognition (FG). pp. 1–11. IEEE (2025)
21. Feichtenhofer, C., Fan, H., Malik, J., He, K.: Slowfast networks for video recognition. In: ICCV. pp. 6202–6211 (2019)
22. fxsjy: <https://github.com/fxsjy/jieba>. In: Github (2020)
23. Giebenhain, S., Kirschstein, T., Rünz, M., Agapito, L., Nießner, M.: Pixel3dmm: Versatile screen-space priors for single-image 3d face reconstruction. arXiv preprint arXiv:2505.00615 (2025)
24. Glauert, J.R., Elliott, R., Cox, S.J., Tryggvason, J., Sheard, M.: Vanessa—a system for communication between deaf and hearing people. In: Technology and disability. vol. 18, pp. 207–216. IOS Press (2006)
25. Guo, C., Zuo, X., Wang, S., Cheng, L.: Tm2t: Stochastic and tokenized modeling for the reciprocal generation of 3d human motions and texts. In: ECCV. pp. 580–597 (2022)
26. Ho, J., Jain, A., Abbeel, P.: Denoising diffusion probabilistic models. In: Advances in Neural Information Processing Systems. vol. 33, pp. 6840–6851 (2020)
27. Hu, H., Zhao, W., Zhou, W., Wang, Y., Li, H.: SignBERT: Pre-Training of Hand-Model-Aware Representation for Sign Language Recognition. In: ICCV. pp. 11087–11096 (2021)
28. Hu, H., Zhou, W., Li, H.: Hand-model-aware sign language recognition. In: AAAI. vol. 35, pp. 1558–1566 (2021)
29. Hu, H., Zhou, W., Pu, J., Li, H.: Global-local enhancement network for NMF-aware sign language recognition. TOMM **17**(3), 1–19 (2021)
30. Huang, W., Pan, W., Zhao, Z., Tian, Q.: Towards fast and high-quality sign language production. In: MM. pp. 3172–3181 (2021)
31. Hwang, E., Kim, J.H., Park, J.C.: Non-autoregressive sign language production with gaussian space. In: BMVC (2021)
32. Ivashechkin, M., Mendez, O., Bowden, R.: Signsplat: Rendering sign language via gaussian splatting. arXiv preprint arXiv:2505.02108 (2025)
33. Jang, Y., Momeni, L., Jiang, Z., Chung, J.S., Varol, G., Zisserman, A.: Lost in translation, found in embeddings: Sign language translation and alignment (2025), <https://arxiv.org/abs/2512.08040>
34. Jiang, B., Chen, X., Liu, W., Yu, J., Yu, G., Chen, T.: Motiongpt: Human motion as a foreign language. NeurIPS **36**, 20067–20079 (2023)
35. Jiang, T., Lu, P., Zhang, L., Ma, N., Han, R., Lyu, C., Li, Y., Chen, K.: Rtmpose: Real-time multi-person pose estimation based on mmpose (2023). <https://doi.org/10.48550/ARXIV.2303.07399>, <https://arxiv.org/abs/2303.07399>
36. Jiao, P., Min, Y., Chen, X.: Visual alignment pre-training for sign language translation. In: ECCV. pp. 349–367. Springer (2024)

37. Karpouzis, K., Caridakis, G., Fotinea, S.E., Efthimiou, E.: Educational resources and implementation of a greek sign language synthesis architecture. *Computers & Education* **49**(1), 54–74 (2007)
38. Kerbl, B., Kopanas, G., Leimkühler, T., Drettakis, G.: 3D Gaussian Splatting for Real-Time Radiance Field Rendering. *ACM Transactions on Graphics (TOG)* **42**(4) (2023)
39. Kingma, D.P., Ba, J.: Adam: A Method for Stochastic Optimization. In: *ICLR* (2015)
40. Kojima, A., Tamura, T., Fukunaga, K.: Natural language description of human activities from video images based on concept hierarchy of actions. *International Journal of Computer Vision* **50**(2), 171–184 (2002)
41. Li, T., Bolkart, T., Black, M.J., Li, H., Romero, J.: Learning a Model of Facial Shape and Expression from 4D Scans. *ACM Transactions on Graphics (TOG)* **36**(6), 1–17 (2017)
42. Li, Z., Zhou, W., Zhao, W., Wu, K., Hu, H., Li, H.: Uni-sign: Toward unified sign language understanding at scale. In: *The Thirteenth International Conference on Learning Representations*
43. Lin, C.Y.: Rouge: A package for automatic evaluation of summaries. In: *Text summarization branches out*. pp. 74–81. Association for Computational Linguistics, Barcelona, Spain (Jul 2004)
44. Lin, J., Gan, C., Han, S.: TSM: Temporal shift module for efficient video understanding. In: *Proceedings of the IEEE/CVF international conference on computer vision*. pp. 7083–7093 (2019)
45. Liu, Y., Gu, J., Goyal, N., Li, X., Edunov, S., Ghazvininejad, M., Lewis, M., Zettlemoyer, L.: Multilingual denoising pre-training for neural machine translation. In: *Transactions of the Association for Computational Linguistics*. vol. 8, pp. 726–742. MIT Press One (2020)
46. Loper, M., Mahmood, N., Romero, J., Pons-Moll, G., Black, M.J.: Smpl: A skinned multi-person linear model. In: *TOG*. vol. 34. ACM New York, NY, USA (2015)
47. Loshchilov, I., Hutter, F.: Decoupled weight decay regularization. In: *ICLR* (2019)
48. McDonald, J., Wolfe, R., Schnepf, J., Hochgesang, J., Jamrozik, D.G., Stumbo, M., Berke, L., Bialek, M., Thomas, F.: An automated technique for real-time production of lifelike animations of american sign language. *Universal Access in the Information Society* **15**, 551–566 (2016)
49. Mentzer, F., Minnen, D., Agustsson, E., Tschannen, M.: Finite scalar quantization: Vq-vae made simple. In: *The Twelfth International Conference on Learning Representations* (2022)
50. Papineni, K., Roukos, S., Ward, T., Zhu, W.J.: Bleu: a method for automatic evaluation of machine translation. In: *ACL*. pp. 311–318 (2002)
51. Pavlakos, G., Choutas, V., Ghorbani, N., Bolkart, T., Osman, A.A., Tzionas, D., Black, M.J.: Expressive body capture: 3d hands, face, and body from a single image. In: *Proceedings of the IEEE/CVF international conference on computer vision*. pp. 10975–10985 (Jun 2019), <http://smpl-x.is.tue.mpg.de>
52. Plappert, M., Mandery, C., Asfour, T.: Learning a bidirectional mapping between human whole-body motion and natural language using deep recurrent neural networks. *Robotics and Autonomous Systems* **109**, 13–26 (2018)
53. Potamias, R.A., Zhang, J., Deng, J., Zafeiriou, S.: Wilor: End-to-end 3d hand localization and reconstruction in-the-wild. In: *Proceedings of the Computer Vision and Pattern Recognition Conference*. pp. 12242–12254 (2025)
54. Qi, F., Duan, Y., Xu, C., Zhang, H.: Signgen: End-to-end sign language video generation with latent diffusion. In: *ECCV* (2024)
55. Qian, S., Kirschstein, T., Schoneveld, L., Davoli, D., Giebenhain, S., Nießner, M.: GaussianAvatars: Photorealistic Head Avatars with Rigged 3D Gaussians. In: *Proceedings of the IEEE/CVF Conference on Computer Vision and Pattern Recognition (CVPR)*. pp. 20299–20309 (2024)

56. Qiu, Z., Yao, T., Mei, T.: Learning spatio-temporal representation with pseudo-3D residual networks. In: Proceedings of the IEEE/CVF international conference on computer vision. pp. 5533–5541 (2017)
57. Raffel, C., Shazeer, N., Roberts, A., Lee, K., Narang, S., Matena, M., Zhou, Y., Li, W., Liu, P.J.: Exploring the limits of transfer learning with a unified text-to-text transformer. *Journal of machine learning research* **21**(140), 1–67 (2020)
58. Razavi, A., Van den Oord, A., Vinyals, O.: Generating diverse high-fidelity images with vq-vae-2. In: Advances in Neural Information Processing Systems. vol. 32 (2019)
59. Rombach, R., Blattmann, A., Lorenz, D., Esser, P., Ommer, B.: High-resolution image synthesis with latent diffusion models. In: CVPR. pp. 10684–10695 (2022), <https://github.com/CompVis/latent-diffusion><https://arxiv.org/abs/2112.10752>
60. Romero, J., Tzionas, D., Black, M.J.: Embodied hands: modeling and capturing hands and bodies together. *TOG* **36**(6), 1–17 (2017)
61. Salvador, S., Chan, P.: Toward accurate dynamic time warping in linear time and space. *Intelligent data analysis* **11**(5), 561–580 (2007)
62. Sáráandi, I., Pons-Moll, G.: Neural localizer fields for continuous 3d human pose and shape estimation. *Advances in Neural Information Processing Systems* **37**, 140032–140065 (2024)
63. Saunders, B., Camgoz, N.C., Bowden, R.: Adversarial training for multi-channel sign language production. *arXiv preprint arXiv:2008.12405* (2020)
64. Saunders, B., Camgoz, N.C., Bowden, R.: Everybody sign now: Translating spoken language to photo realistic sign language video. In: *arXiv preprint arXiv:2011.09846* (2020)
65. Saunders, B., Camgoz, N.C., Bowden, R.: Progressive transformers for end-to-end sign language production. In: *European Conference on Computer Vision*. pp. 687–705. Springer (2020)
66. Saunders, B., Camgoz, N.C., Bowden, R.: Mixed signals: Sign language production via a mixture of motion primitives. In: *Proceedings of the IEEE/CVF International Conference on Computer Vision*. pp. 1919–1929 (2021)
67. Song, Y., Sohl-Dickstein, J., Kingma, D.P., Kumar, A., Ermon, S., Poole, B.: Score-based generative modeling through stochastic differential equations. *arXiv preprint arXiv:2011.13456* (2020)
68. Stokoe, W.C.: Sign language structure. *Annual Review of Anthropology* **9**, 365–390 (1980). <https://doi.org/10.1146/annurev.an.09.100180.002053>, <https://www.annualreviews.org/content/journals/10.1146/annurev.an.09.100180.002053>
69. Stoll, S., Camgoz, N.C., Hadfield, S., Bowden, R.: Text2sign: towards sign language production using neural machine translation and generative adversarial networks. *International Journal of Computer Vision* **128**(4), 891–908 (2020)
70. Stoll, S., Mustafa, A., Guillemaut, J.Y.: There and back again: 3d sign language generation from text using back-translation. In: *2022 International Conference on 3D Vision (3DV)*. pp. 187–196. IEEE (2022)
71. Sutton-Spence, R., Woll, B.: *The linguistics of British Sign Language: an introduction*. Cambridge University Press (1999)
72. Symeonidis-Herzig, A., Sincan, O.M., Bowden, R.: Visualspeaker: Visually-guided 3d avatar lip synthesis. In: *Proceedings of the IEEE/CVF International Conference on Computer Vision (ICCV) Workshops*. pp. 6666–6675 (Oct 2025)
73. Takano, W., Nakamura, Y.: Statistical mutual conversion between whole body motion primitives and linguistic sentences for human motions. *The International Journal of Robotics Research* **34**(10), 1314–1328 (2015)
74. Tang, S., Hong, R., Guo, D., Wang, M.: Gloss semantic-enhanced network with online back-translation for sign language production. In: *Proceedings of the 30th ACM International Conference on Multimedia*. pp. 5630–5638 (2022)

75. Tevet, G., Raab, S., Gordon, B., Shafir, Y., Bermano, A.H., Cohen-Or, D.: Human motion diffusion model. arXiv preprint arXiv:2209.14916 (2022)
76. Uthus, D., Tanzer, G., Georg, M.: YouTube-ASL: A Large-Scale, Open-Domain American Sign Language-English Parallel Corpus (2023)
77. Van Den Oord, A., Vinyals, O.: Neural Discrete Representation Learning. *Advances in Neural Information Processing Systems* **30** (2017)
78. Vaswani, A., Shazeer, N., Parmar, N., Uszkoreit, J., Jones, L., Gomez, A.N., Kaiser, Ł., Polosukhin, I.: Attention is all you need. *Advances in neural information processing systems* **30**, 5998–6008 (2017)
79. Walsh, H., Ivashechkin, M., Bowden, R.: Using sign language production as data augmentation to enhance sign language translation. In: *Adjunct Proceedings of the 25th ACM International Conference on Intelligent Virtual Agents*. pp. 1–10 (2025)
80. Walsh, H., Ravanshad, A., Rahmani, M., Bowden, R.: A data-driven representation for sign language production. In: *Proceedings of the 18th International Conference on Automatic Face and Gesture Recognition*. pp. 1–10. IEEE (2024)
81. Wang, C., Deng, Z., Jiang, Z., Shen, F., Yin, Y., Gan, S., Cheng, Z., Ge, S., Gu, Q.: Advanced sign language video generation with compressed and quantized multi-condition tokenization (2025), <https://arxiv.org/abs/2506.15980>
82. Wang, K., Wu, Q., Song, L., Yang, Z., Wu, W., Qian, C., He, R., Qiao, Y., Loy, C.C.: MEAD: A Large-Scale Audio-Visual Dataset for Emotional Talking-Face Generation. In: *Proceedings of the European Conference on Computer Vision (ECCV)* (2020)
83. Wang, Y., Huang, D., Zhang, Y., Ouyang, W., Jiao, J., Feng, X., Zhou, Y., Wan, P., Tang, S., Xu, D.: Motiongpt-2: A general-purpose motion-language model for motion generation and understanding. arXiv preprint arXiv:2410.21747 (2024)
84. Wei, F., Chen, Y.: Improving continuous sign language recognition with cross-lingual signs. In: *Proceedings of the IEEE/CVF international conference on computer vision*. pp. 23612–23621 (Oct 2023)
85. Wong, R., Camgoz, N.C., Bowden, R.: Sign2GPT: Leveraging large language models for gloss-free sign language translation. In: *ICLR* (2024)
86. Wong, R., Camgoz, N.C., Bowden, R.: Signrep: Enhancing self-supervised sign representations. In: *Proceedings of the IEEE/CVF international conference on computer vision* (2025), <https://arxiv.org/abs/2503.08529>
87. Xin, C., Jiang, B., Liu, W., Huang, Z., Fu, B., Chen, T., Yu, J., Yu, G.: Executing your commands via motion diffusion in latent space. In: *Proceedings of the IEEE/CVF Conference on Computer Vision and Pattern Recognition (CVPR)* (Jun 2023)
88. Yan, S., Xiong, Y., Lin, D.: Spatial temporal graph convolutional networks for skeleton-based action recognition. In: *AAAI* (2018)
89. Yang, Z., Zeng, A., Yuan, C., Li, Y.: Effective whole-body pose estimation with two-stages distillation. In: *Proceedings of the IEEE/CVF International Conference on Computer Vision*. pp. 4210–4220 (2023)
90. Yin, A., Li, H., Shen, K., Tang, S., Zhuang, Y.: T2S-GPT: Dynamic Vector Quantization for Autoregressive Sign Language Production from Text. In: *ACL* (2024)
91. Zhang, D., Liu, Y., Lin, L., Zhu, Y., Li, Y., Qin, M., Li, Y., Wang, H.: GUAVA: Generalizable Upper-Body 3D Gaussian Avatars. arXiv preprint arXiv:2505.03351 (2025)
92. Zhang, J., Zhang, Y., Cun, X., Zhang, Y., Zhao, H., Lu, H., Shen, X., Shan, Y.: Generating human motion from textual descriptions with discrete representations. In: *CVPR*. pp. 14730–14740 (2023)
93. Zhang, M., Cai, Z., Pan, L., Hong, F., Guo, X., Yang, L., Liu, Z.: Motiondiffuse: Text-driven human motion generation with diffusion model. *IEEE transactions on pattern analysis and machine intelligence* **46**(6), 4115–4128 (2024)

94. Zhao, W., Hu, H., Zhou, W., Shi, J., Li, H.: BEST: Bert pre-training for sign language recognition with coupling tokenization. In: AAAI. vol. 37, pp. 3597–3605 (2023)
95. Zhou, H., Zhou, W., Qi, W., Pu, J., Li, H.: Improving sign language translation with monolingual data by sign back-translation. In: CVPR. pp. 1316–1325 (2021)
96. Zhou, W., Zhao, W., Hu, H., Li, Z., Li, H.: Scaling up multimodal pre-training for sign language understanding. *IEEE Transactions on Pattern Analysis and Machine Intelligence* (2025)
97. Zhou, Y., Barnes, C., Lu, J., Yang, J., Li, H.: On the continuity of rotation representations in neural networks. In: Proceedings of the IEEE/CVF conference on computer vision and pattern recognition. pp. 5745–5753 (2019)
98. Zuo, R., Potamias, R.A., Ververas, E., Deng, J., Zafeiriou, S.: Signs as tokens: A retrieval-enhanced multilingual sign language generator (2025), <https://arxiv.org/abs/2411.17799>
99. Zuo, R., Wei, F., Mak, B.: Natural language-assisted sign language recognition. In: Proceedings of the IEEE/CVF international conference on computer vision. pp. 14890–14900 (2023)

Supplementary Material for M³T: Discrete Multi-Modal Motion Tokens for Sign Language Production

This appendix provides additional technical details, analyses, and visualizations. Section A includes extended qualitative results alongside a user study evaluating perceived sign quality. Section B analyses the motion vocabulary statistics across modalities. Section C expands on the foundations of SMPL-FX with a detailed formulation of the hybrid body–face representation. Section D presents comprehensive implementation and training details to facilitate reproducibility.

A Additional Qualitative Results

The extended qualitative examples (Fig. A.1) show M³T’s expressive and accurate signing over longer sequences. Across all three datasets, the generated sequences exhibit coordinated NMFs: mouth shapes vary in synchrony with manual signs, and eyebrow movements align with interrogative or emphatic contexts. The temporal coherence of body posture and hand configurations is maintained even over multi-sentence utterances, without the drift or freezing artifacts common in long autoregressive generation.

A.1 User Study

We conduct a pairwise preference study comparing M³T against SOKE [98]. Participants were shown six randomized video pairs spanning all three datasets and asked which sequence they preferred on two axes: facial expressivity and overall motion quality. As our evaluation covers three sign languages (ASL, CSL, DGS), participants assessed perceived naturalness and expressivity. Results (Fig. A.2) show a clear preference for M³T: participants favored our generations in 68.8% of comparisons for facial expressivity and 64.6% for overall quality, consistent with SMPL-FX’s richer expression space and FSQ’s higher codebook utilization. Lip articulation was identified as the most common weakness, consistent with the monocular fitting limitations discussed in Sec. C. Participants also noted that generated motion tends to occupy a smaller signing space than real signing, likely due to temporal compression in the tokenization stage.

B Statistics on Sign Motion Vocabulary

We visualize the token frequency distribution across all test sets in Fig. A.3. For comparison, we include the distribution obtained from a VQ-based VAE with an identical codebook size. Unlike VQ, which often exhibits pronounced frequency spikes for individual tokens across multiple configurations, FSQ produces a more balanced utilization of the codebook. This uniformity is evident in the visualization and further supported by the modality-specific standard deviations reported in Table A.2.



Fig. A.1: Additional Qualitative Results. Extended sequences from M³T on How2Sign (top), CSL-Daily (middle), and Phoenix14T (bottom). Note the variation in facial expressions across frames, with mouth movements and eyebrow raises coordinated with the manual signs. Body posture and hand configurations maintain temporal coherence over these longer sequences.

C SMPL-FX

This section details the SMPL-FX body model summarized in the main paper. We first review the shared 3DMM formulation before describing the FLAME integration and

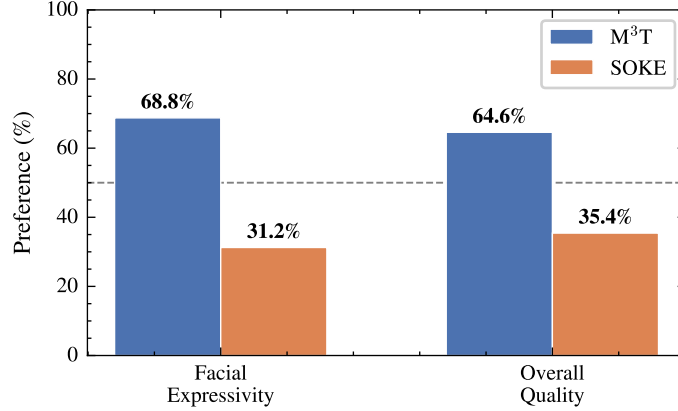


Fig. A.2: User study results. Preference rates (%) for facial expressivity and overall motion quality, comparing M³T against SOKE [98] (6 video pairs).

per-frame fitting pipeline. Figure 2 in the main paper compares expressions reconstructed with baseline SMPL-X parameters from [98] against our SMPL-FX fitting, showing that SMPL-FX preserves NMFs that SMPL-X cannot.

3DMM Preliminaries. Parametric models such as SMPL [46], MANO [60], and FLAME [41] are widely used 3DMMs [5] that share a mesh generation formulation:

$$\mathbf{M}(\boldsymbol{\beta}, \boldsymbol{\theta}, \boldsymbol{\psi}) = W(T_P(\boldsymbol{\beta}, \boldsymbol{\theta}, \boldsymbol{\psi}), J(\boldsymbol{\beta}), \boldsymbol{\theta}, \mathbf{W}), \quad (\text{A.1})$$

where $W(\cdot)$ applies linear blend skinning to a template mesh $\bar{\mathbf{T}}$ using learned blend weights \mathbf{W} and joint locations $J(\boldsymbol{\beta})$. The rest-pose mesh is given by:

$$T_P(\boldsymbol{\beta}, \boldsymbol{\theta}, \boldsymbol{\psi}) = \bar{\mathbf{T}} + B_S(\boldsymbol{\beta}) + B_P(\boldsymbol{\theta}) + B_E(\boldsymbol{\psi}), \quad (\text{A.2})$$

where B_S , B_P , and B_E model identity, articulation, and expression. Only FLAME and SMPL-X [51] include expression blendshapes B_E . Table A.1 compares mesh vertex counts and parameter spaces across all relevant models.

Formulation. SMPL-FX inherits from SMPL-X and replaces its head region with a FLAME mesh. A precomputed vertex correspondence map identifies which SMPL-X vertices correspond to FLAME vertices. At initialization, the SMPL-X template vertices at those indices are replaced with FLAME’s template geometry, offset by the mean displacement to preserve global alignment. FLAME’s shape and expression blendshape directions are then retargeted into full-body buffers: each buffer has the dimensionality of the SMPL-X mesh but is non-zero only at the FLAME-corresponding indices. SMPL-X’s own shape blendshapes are zeroed at the same indices so that body shape does not deform the face. To avoid a visible seam at the neck boundary, vertex blendshape weights are linearly interpolated across concentric neck rings defined by FLAME’s topology: ratios decay from 0.9 (outermost ring, closest to the body) to 0.1 (innermost, closest to the jaw), smoothly transitioning between SMPL-X and FLAME influence. During the forward pass, FLAME shape and expression blendshapes are applied first, followed by

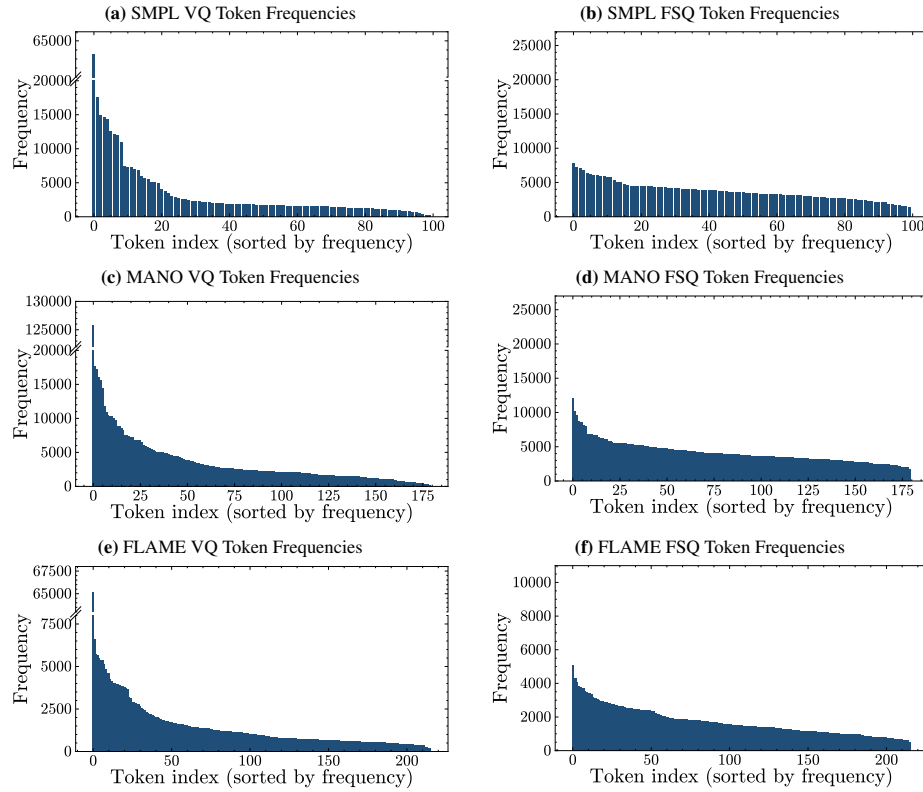


Fig. A.3: Token frequency distributions for body (SMPL), hand (MANO), and face (FLAME) modalities. VQ produces skewed distributions; FSQ yields more uniform coverage across all modalities. The FLAME distributions are also shown in the main paper (Fig. 5) alongside the ablation discussion.

optional eyelid displacements [23] (two per-vertex offset buffers scaled by scalar eyelid parameters). SMPL-X body-shape blendshapes (with the face zeroed out) are then added, and standard linear blend skinning is applied using SMPL-X’s joint regressor and blend weights. Teeth are added as rigid geometry attached to the jaw and lower-jaw joints, inheriting their transformations from the skinning step [55]. The final SMPL-FX mesh comprises 10,995 vertices and 42 pose joints, the latter retaining FLAME’s eye joints while discarding 11 lower-body joints unused in sign production. The face parameter vector ψ_f is 108-dimensional: 100 FLAME expression coefficients, 2 eyelid parameters, and 6 jaw pose parameters (one joint in the 6D rotation representation [97]).

Extraction Pipeline. Fitting all SMPL-FX parameters jointly from monocular video is difficult because expression blendshapes produce small vertex displacements that are easily dominated by body pose. Each modality is therefore extracted with a dedicated tracker—NLF [62] for body, WiLoR [53] for hands, and Pixel3DMM [23] for face—then

fused and refined via joint optimization. The loss combines three terms:

$$\mathcal{L}_{\text{fit}} = \lambda_{\text{kp}}\mathcal{L}_{\text{kp}} + \lambda_{\text{acc}}\mathcal{L}_{\text{acc}} + \lambda_{\text{reg}}\mathcal{L}_{\text{reg}}, \quad (\text{A.3})$$

where \mathcal{L}_{kp} is an L2 reprojection loss against 2D keypoints from RTMPose [15,35] ($\lambda_{\text{kp}} = 1.0$), \mathcal{L}_{acc} penalizes vertex acceleration for temporal smoothness ($\lambda_{\text{acc}} = 0.5$), and \mathcal{L}_{reg} regularizes pose and expression parameters toward the per-tracker initialization ($\lambda_{\text{reg}} = 0.01$). Optimization is performed per clip using Adam on an RTX 3090. While SMPL-FX substantially increases facial expressivity over SMPL-X, mesh quality is ultimately bounded by the upstream monocular fitting stage, where lip detail is particularly difficult to recover from a single viewpoint. This limitation propagates through the full pipeline, since the FSQ-VAE can only tokenize what the fitting provides and the production model can only generate what the tokenizer encodes. Feedback from our user study (Sec. A.1) corroborates this, with participants identifying lip articulation as a common weakness.

Model	Vertices	Parameters		
		Shape	Pose	Expr.
SMPL [46]	6,890	10	21	–
MANO [60]	778	10	15	–
FLAME [41]	5,023	300	4	100
SMPL-X [51]	10,475	10	54	10
<i>SMPL-FX</i>	10,995	310	42	102

Table A.1: Mesh resolution and parameter dimensions. SMPL-FX enhances SMPL-X’s head with FLAME’s expression space, removing joints irrelevant to signing.

	SMPL	MANO	FLAME
VQ SD	6,964	9,658	4,499
FSQ SD	1,316 _{↓81%}	1,605 _{↓83%}	842 _{↓81%}

Table A.2: Standard deviation of token counts across SMPL-FX modalities. FSQ yields $\approx 82\%$ lower SD than VQ, indicating more uniform codebook utilization.

D Implementation and Training Details

The following sections detail the architecture and training procedures for all components: the FSQ-VAEs (Sec. D.1), the Sign Motion Language Model (Sec. D.2), the Sign Language Recognition model (Sec. D.3), and the Back-Translation models (Sec. D.4).

D.1 Multi-Modal Sign Motion Tokenization

Our per-modality motion FSQ-VAEs build upon the VAEs introduced in MotionGPT [34]. As noted in Table 3, certain configurations yield marginally improved reconstructions for specific modalities; however, a shared encoder architecture is used across all three. Each encoder $\mathcal{E}_m(\cdot)$ (Eq. (3)) begins with a Conv1D layer mapping inputs to an internal width of 1024, followed by 2 downsampling stages (Conv1D with stride 2), each

paired with a ResNet-1D stack of six residual blocks. These blocks employ dilated convolutions with a dilation growth rate of 3. A final Conv1D reduces channels to 3 for the latent representation. The decoders $\mathcal{D}_m(\cdot)$ (Eq. (5)) mirror this structure with reversed dilation and nearest-neighbor upsampling replacing strided convolutions. For quantization, we adopt FSQ [49], which introduces no learnable parameters and is configured via the predefined number of levels per dimension. The codebook size is given by $C_m = \prod_{i=1}^d L_m^i$, where L_m^i denotes the number of levels for dimension i in modality m . We select L per modality to achieve codebook sizes comparable to SOKE [98], resulting in $L_b = \{5, 5, 4\}$, $L_h = \{6, 6, 5\}$, and $L_f = \{6, 6, 6\}$ for body, hands, and face, respectively. Each FSQ-VAE comprises approximately 120M parameters, split nearly evenly between encoder and decoder.

Training Setup. Training is performed on a single NVIDIA RTX 3090 GPU using the Adam optimizer [39] with a learning rate of 10^{-4} for 100 epochs and a batch size of 8. We employ cosine annealing with a 25-epoch warm-up and a minimum learning rate of 10^{-6} . Training uses an L2 reconstruction loss on SMPL-FX parameters and we select the checkpoint with the lowest validation vertex reconstruction error per modality.

D.2 Sign Motion Language Model

The SMLM is built on mBART-large-cc25 [45], following the architecture of MotionGPT [34] and incorporating adaptations inspired by SOKE [98]. The mBART encoder–decoder remains unchanged, preserving its 12 layers and 1024-dimensional hidden size. To handle multimodal motion data, we extend mBART’s tokenizer (Eq. (7)) with a motion-specific vocabulary and introduce 5 modality-specific token prediction heads: text, body, left hand, right hand, and face. Each head is implemented as a linear layer mapping the shared hidden representation to the respective vocabulary indices. During input token fusion, modality embeddings are combined via equal-weight averaging. The complete model comprises 396M parameters.

Training Setup. Our SMLM is trained on two NVIDIA RTX 3090 GPUs using the AdamW optimizer [47]. A cosine annealing learning rate schedule is employed, starting at 2×10^{-4} and decaying to 10^{-6} . Training spans 200 epochs at a batch size of 32, completing within 4 days. The objective is cross-entropy loss, and the best checkpoint is selected based on mean DTW-MJPE performance on the validation set of all datasets.

D.3 Sign Language Recognition

Our SLR module leverages the pose encoder’s intermediate representations, specifically the 1024-dimensional hidden states extracted prior to quantization. These per-modality features are interleaved into a structured sequence $\{\text{body}, \text{hand_l}, \text{hand_r}, \text{face}, \dots\}$ which is processed by a 3-layer Transformer encoder with a hidden size of 1024 and 4 attention heads. The output is passed through an MLP classifier. The additional recognition stack introduces 26M parameters on top of the frozen encoder from the tokenizer described in Sec. D.1.

Training Setup. The SLR model is trained on a single NVIDIA RTX 3090 GPU using the Adam optimizer [39]. We employ a cosine annealing schedule starting at 2×10^{-4}

and decaying to 10^{-6} . Training runs for 100 epochs with a batch size of 64, completing in 12 hours. The loss function is cross-entropy with label-smoothing ($\alpha = 0.1$). The final checkpoint is selected based on the best top-1 accuracy across the validation set.

D.4 Back-Translation Model

Our back-translation model builds upon the publicly available Sign Language Transformer (SL-T) [9], following the progressive training approach of [65]. We adapt the base implementation to accommodate SMPL-FX input modalities, concatenating all features into a 360-dimensional input vector. The original CNN-based feature extractor is removed, allowing the model to directly process 6D pose and facial expressions.

Because SL-T was originally designed exclusively for Phoenix14T [7], which is German and includes gloss² annotations, modifications were required for other datasets. For CSL-Daily, which contains Chinese text, SL-T’s character- or word-level tokenizer is incompatible; we address this by employing Jieba [22] for segmentation. For How2Sign [18], which lacks gloss annotations, we generate pseudo-glosses³ based on part-of-speech tags using the method introduced in Sign2GPT [85].

Training Setup. Models are trained separately for each sign language using an NVIDIA RTX 3090 GPU. We employ the Adam optimizer [39] with a learning rate of 2.5×10^{-4} and a batch size of 256 (128 for How2Sign due to longer sequences). A plateau-based scheduler reduces the learning rate when validation performance stagnates, with a patience of 10 and a decay factor of 0.8. Training completes in under one day for Phoenix14T and CSL-Daily, while How2Sign requires more than twice the time due to increased sequence lengths. We select the checkpoint achieving the highest validation BLEU-4 score and use this model for back-translation inference to evaluate the SMLM.

²A gloss is a written approximation of a sign’s meaning.

³A pseudo-gloss is an automatically generated approximation of a sign’s meaning, often derived from the written translation.